NEURAL REGENERATION RESEARCH
www.nrronline.org

Research Article

Sustained delivery of vascular endothelial growth factor mediated by bioactive methacrylic anhydride hydrogel accelerates peripheral nerve regeneration after crush injury

https://doi.org/10.4103/1673-5374.335166

Date of submission: May 31, 2021

Date of decision: August 31, 2021

Date of acceptance: November 9, 2021

Date of web publication: February 8, 2022

Wanlin Xu[1, #], Yifan Wu[1, #], Hao Lu[1], Yun Zhu[1], Jinhai Ye[2, *], Wenjun Yang[1, *]

From the Contents

Graphical Abstract *Injection of vascular endothelial growth factor-loaded hydrogel promotes peripheral nerve regeneration*

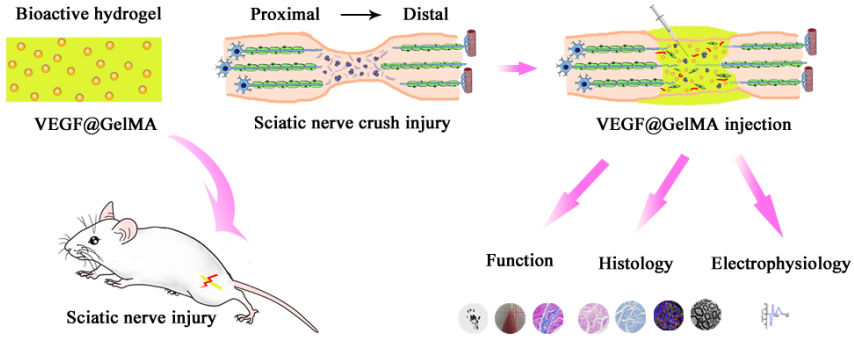

Abstract

Neurotrophic factors, currently administered orally or by intravenous drip or intramuscular injection, are the main method for the treatment of peripheral nerve crush injury. However, the low effective drug concentration arriving at the injury site results in unsatisfactory outcomes. Therefore, there is an urgent need for a treatment method that can increase the effective drug concentration in the injured area. In this study, we first fabricated a gelatin modified by methacrylic anhydride hydrogel and loaded it with vascular endothelial growth factor that allowed the controlled release of the neurotrophic factor. This modified gelatin exhibited good physical and chemical properties, biocompatibility and supported the adhesion and proliferation of RSC96 cells and human umbilical vein endothelial cells. When injected into the epineurium of crushed nerves, the composite hydrogel in the rat sciatic nerve crush injury model promoted nerve regeneration, functional recovery and vascularization. The results showed that the modified gelatin gave sustained delivery of vascular endothelial growth factors and accelerated the repair of crushed peripheral nerves.

Key Words: bioactive material; controlled release; crush injury; hydrogel; muscle function; nerve regeneration; peripheral nerve; sciatic function index; vascular endothelial growth factor; vascularization

Introduction

Peripheral nerve injury (PNI) occurs in about 3% of trauma patients around the world (Li et al., 2021a). It may result in total or partial loss of sensory and motor function, leading to a succession of dysfunctions, including sensation loss, neuropathic pain, muscle atrophy and paralysis, which can have substantial social and labor impacts. Sir Sydney Sunderland (1951) first classified five grades of PNI based on the discontinuity of several layers of connective tissues (specifically, the endoneurium, perineurium, and epineurium). According to Sunderland's classifications, crush injury belongs to grade 4 (there is only continuity of the epineurium, whereas there is discontinuity in all other layers, including the axonal sheath) (Flores et al., 2000). Clearly, it is much more severe than injuries from grades 1 to 3 crushes and requires more therapeutic attention than lower grade injuries.

In contrast to the central nervous system, the peripheral nervous system (PNS) has some self-repair capacity, which is partially due to the abundance of extracellular matrix components in its basal lamina (Li et al., 2021a). However, the regeneration capacity of the PNS may be restricted by various factors, including age, injury sites, and injury severity (Ruijs et al., 2005). Thus, many strategies have been tried to improve the ability to repair damage sustained by crush injury, including combination treatments using erythropoietin and dexamethasone (Lee et al., 2020), wrapping the injury site

[1]Department of Oral and Maxillofacial-Head and Neck Oncology, Shanghai Ninth People's Hospital, Shanghai Jiao Tong University School of Medicine; College of Stomatology, Shanghai Jiao Tong University; National Center for Stomatology; National Clinical Research Center for Oral Diseases; Shanghai Key Laboratory of Stomatology, Shanghai, China; [2]Jiangsu Key Laboratory of Oral Diseases, Department of Oral and Maxillofacial Surgery, The Affiliated Stomatological Hospital of Nanjing Medical University, Nanjing, Jiangsu Province, China

*Correspondence to: Wenjun Yang, PhD, 450907991@qq.com; Jinhai Ye, PhD, jhyeedoctor@163.com.

https://orcid.org/0000-0002-3291-8153 (Wanlin Xu)

#Both authors contributed equally to this article.

Funding: *This work was supported by the Interdisciplinary Program of Shanghai Jiao Tong University, China, No. YG2021QN60 (both to WL); and Fundamental Research Program Funding of Ninth People's Hospital Affiliated to Shanghai Jiao Tong University School of Medicine, China, No. JYZZ086B (both to WL).*

How to cite this article: *Xu W, Wu Y, Lu H, Zhu Y, Ye J, Yang W (2022) Sustained delivery of vascular endothelial growth factor mediated by bioactive methacrylic anhydride hydrogel accelerates peripheral nerve regeneration after crush injury. Neural Regen Res 17(9):2064-2071.*

with scaffold-free dental pulp cell sheets (Ahmed et al., 2021), transplantation of Schwann cell-like cell spheroids (Lin et al., 2020), among others. Recently, Lopez-Silva et al. (2021) used an auto nanoliter injector with a glass needle to apply multidomain peptide hydrogels into an injury site. They effectively enhanced neurite outgrowth and elicited beneficial responses indicating peripheral nerve regeneration. Therefore, we postulated that direct administration of other biological facilitators through microinjection might help to accelerate nerve repair after peripheral nerve crush injury.

Vascular endothelial growth factor (VEGF) is a multifunctional growth factor that has main functions in vascularization and angiogenesis (Ferrara et al., 2003). In our previous study, VEGF was confirmed to be beneficial for critical bone defect repair (Xu et al., 2017). VEGF also has some neuroprotective and neurotrophic effects that include neuron survival and improving neurite outgrowth. The delivery of VEGF promoted both the maintenance and regrowth of damaged axons in mice by regulating the expression of glial-derived neurotrophic factors and nerve growth factors (Shvartsman et al., 2014). Others showed that trophic sensory and functions can be restored and injured peripheral neurons can be selectively regenerated by VEGF-B (Guaiquil et al., 2014). This suggests that VEGF-B would be an appropriate therapeutic target for treating PNI. However, direct use of VEGF has several drawbacks, such as burst release phenomenon, a short *in vivo* half-life and subsequent off-target effects (Henry et al., 2003). Thus, achieving a controlled delivery of VEGF is of particular importance in tissue engineering and regeneration.

To realize the sustained delivery of biochemical cues, it has been shown that a promising strategy was using bioactive hydrogels (Lu et al., 2019; Raimondo et al., 2019; Liu et al., 2020; Qiao et al., 2020; Li et al., 2021b). Gelatin modified by methacrylic anhydride (GelMA) hydrogel has attracted the attention of many researchers because of its excellent biocompatibility and its similarities to the natural extracellular matrix (Fan et al., 2018; Dursun Usal et al., 2019). GelMA hydrogel has been reported to be one of the best carriers for the controllable release of growth factors or drugs, such as human basic fibroblast growth factor (Luo et al., 2021), puerarin (Qin et al., 2020) and aspirin (Liu et al., 2021).

In this study, we hypothesized that administration of VEGF-laden GelMA hydrogel directly into a crushed sciatic nerve would promote its functional recovery, reinnervation and vascularization. To confirm this, VEGF165 (a VEGF-A isoform) was incorporated into GelMA, to form VEGF@GelMA hydrogel, to achieve a controlled release of this multifunctional growth factor. Initially, the compatibility of the hydrogel and bioactivity of the hydrogel leachate were investigated *in vitro*. Finally, the neurogenesis and angiogenesis capacities of this VEGF-laden GelMA hydrogel were evaluated in an established crush injury model of rat sciatic nerves (**Figure 1**).

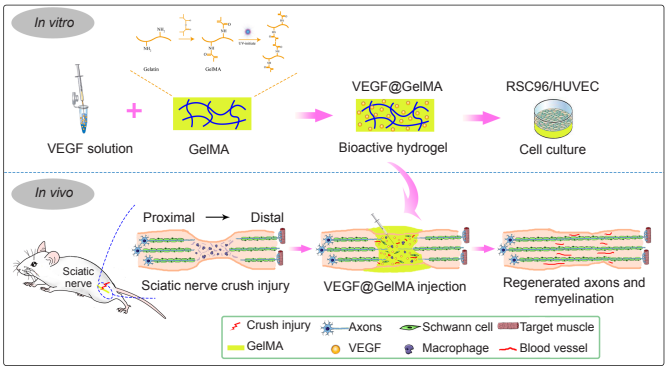

Figure 1 | **Bioactive hydrogel (VEGF@GelMA) accelerates peripheral nerve regeneration after crush injury.**
GelMA: Gelatin modified by methacrylic anhydride; HUVEC: human umbilical vein endothelial cells; VEGF: vascular endothelial growth factor.

Materials and Methods

Hydrogel fabrication and investigation

Construction of the bioactive hydrogel

The gelatin methacrylate (GelMA; GM-60, Engineering For Life, Suzhou, China) hydrogel was fabricated as per the instructions of manufacturer (Hu et al., 2020). Briefly, lithium phenyl-2,4,6-trimethylbenzoylphosphinate photo-initiator was first dissolved in phosphate buffered saline (PBS; 0.1%, w/v, pH 7.0), while in a water bath, and the solution was heated to 60°C for 30 minutes. Next, the dried GelMA was dissolved in lithium phenyl-2,4,6-trimethylbenzoylphosphinate solution to form a 5%, w/v uncrosslinked GelMA solution. The GelMA hydrogel was then crosslinked by irradiating the solution with a blue-violet light source (405 nm, 3 W) for 20 seconds for use in subsequent experiments. For the VEGF@GelMA hydrogel fabrication, recombinant human VEGF165 (Peprotech, Cranbury, NJ, USA) was dissolved in an uncrosslinked GelMA solution at a concentration of 0.2 μg/mL and subsequently irradiated as above.

Hydrogel observation

After freeze drying with the freeze dryer, the uncrosslinked and crosslinked GelMA samples were fixed on specimen platforms. The samples were sputter coated with a gold protective film and then observed under a scanning electron microscope (Zeiss Gemini 300, Oberkochen, Germany).

Fourier transform infrared spectrometry analysis

For Fourier transform infrared spectrometry, the uncrosslinked and crosslinked GelMA hydrogels were dried in the freeze dryer, grounded into fine powder and then pelletized with potassium bromide (KBr) to form a transparent sheet. The spectra were recorded for Fourier transform infrared spectrometry analysis over the wavenumber range from 400 to 4000 cm^{-1} using a spectrometer (1600, PerkinElmer Co., Boston, MA, USA)..

Degeneration of the hydrogel

To evaluate the degeneration rate of the hydrogel, the hydrogel was soaked for 1 day in PBS to achieve the W_0 state (i.e., equilibrium swelling state). Then a degeneration test was conducted at 37°C in collagenase-2 (MilliporeSigma, Burlington, MA, USA) solution (2 U/mL). At subsequent time points (1, 2, 3, 4, 5 and 6 hours), the remaining gel mass was weighed and recorded as W_t. The degeneration rate was tracked using the following formula: Degeneration rate (%) = $(W_0 - W_t)/W_0 \times 100$ (Liu et al., 2021).

Swelling property of the hydrogel

The swelling property of this bioactive hydrogel was determined as follows. The primary weight of the dried hydrogel was logged as W_0. It was weighed again after the 1 day immersion of the hydrogel in PBS at room temperature. The hydrogel weight was measured and logged as W_t. The following formula is used for calculating the swelling ratio: Swelling ratio (%) = $(W_t - W_0)/W_0 \times 100$ (Liu et al., 2021).

VEGF release kinetics of bioactive hydrogel

The release kinetics of VEGF@GelMA were measured as previously described (Xu et al., 2017). Briefly, the VEGF@GelMA hydrogel was soaked in PBS for various periods of time. At set time points, 0.5 mL medium was sampled and an equal amount of fresh PBS was added to replace it. The amount of VEGF released into the medium was detected using an ELISA Kit (R&D System, Minneapolis, MN, USA) as per the instructions of manufacturer. The release kinetics were calculated using the following formula: $m_t = m_1 + m_2 + m_3 + \ldots\ldots + m_x$, where m_x indicates the released amount measured at time x, and m_t refers to the cumulative amount of released VEGF protein.

Cell culture

Both human umbilical vein endothelial cells (HUVECs; RRID: CVCL_2959) and RSC96 Schwann cells (RRID: CVCL_4694) were purchased from the Cell Bank, Chinese Academy of Sciences (Shanghai, China). The RSC96 cells were cultured in high-glucose Dulbecco's modified Eagle medium (Hyclone, Logan City, UT, USA) with 1% streptomycin/penicillin (Solarbio, Beijing, China) solution and 10% fetal bovine serum (Gibco-AUS, Thornton, Australia). The HUVECs were cultured in endothelial cell growth medium-2 medium (Lonza, Walkersville, MD, USA). All cells were cultured in a humidified incubator (Thermo Scientific, Waltham, MA, USA) at 37°C with 95% air and 5% CO_2. To test the biocompatibility of the GelMA hydrogel, equal weights (or volumes) of RSC96 cells and GelMA hydrogel were mixed. The HUVECs were then seeded on the surface of the gel and immediately irradiated with ultraviolet. RSC96 cells and HUVECs cultured on tissue culture polystyrene (TCP) (Corning, Corning, NY, USA) were used as a control.

Animals and surgical process

This study evaluating the therapeutic effects of the above bioactive

hydrogels was approved by Institutional Animal Care and Use Committee of School of Medicine, Shanghai Jiao Tong University (Shanghai, China; approval No. SH9H-2020-A762-1) on November 11, 2020. All experiments were designed and reported according to the Animal Research: Reporting of *In Vivo* Experiments (ARRIVE) guidelines (Kilkenny et al., 2011). A single surgeon (WLX) performed all the surgery and injection procedures to minimize operation bias. Forty-eight male specific-pathogen-free Sprague-Dawley rats (weighing 200–220 g, aged 6–8 weeks) were randomly divided into four groups: sham, crush + PBS, crush + GelMA and crush + VEGF@GelMA groups (n =12 for each group). The peripheral sciatic nerve crush injury model used was as follows. After the rats were anesthetized with 2% pentobarbital sodium (50 mg/kg body weight; Sigma, Shanghai, China), the sciatic nerve of the left leg was uncovered and dissected carefully by means of a gluteal splitting method following instructions in previous studies (Beer et al., 2001; Varejão et al., 2004). The middle part of the exposed nerve was intercross crushed with 5-inch hemostatic forceps (Jinzhong, Shanghai, China) at three clicks for 20 seconds. These rats were all designated as crush groups. Then, for rats in crush + PBS, crush + GelMA and crush + VEGF@GelMA groups, 2 μL PBS, or an equal amount of 5% (w/v) GelMA or VEGF@GelMA, was gradually injected into the epineurium of the crushed nerve and surrounding tissues at the middle of crushed site. A 9-0 nylon suture (Ethicon, Somerville, NJ, USA) was used to mark the injury site at the crush injury's proximal end. After closing the muscle and then the skin, all animals were returned to their cages where they could move freely and have free access to water and food. The right leg was set as the contralateral (normal control) side. For the sham group, the sciatic nerve was exposed without crush injury.

Immunofluorescence staining

Standard protocol was used for the immunofluorescent staining of RSC96 or HUVEC cells or slices of paraffin embedded sciatic nerve tissues 4 weeks after surgery. Briefly, rats were anesthetized by intraperitoneal injection with pentobarbital sodium (0.05 mg/g body weight). The sciatic nerves were exposed and the nerve samples were fixed with 4% paraformaldehyde, 0.2% Triton X-100 for permeabilization, then sealed with bovine serum albumin (Yeason, Shanghai, China) and incubated with phalloidin or a selected primary antibody. To observe cell morphology and attachment, HUVECs or RSC96 cells were then stained with 100 nM phalloidin (Yeason), an actin filament stain. The nerve tissues were incubated with rabbit anti-S100β (1:1000; Cat# ab41548, RRID: AB_2184443, Abcam, Cambridge, MA, USA), rabbit anti-myelin basic protein (1:1000, Cat# ab40390, RRID: AB_1141521, Abcam), rabbit anti-neurofilament-200 (1:1000, Cat# ab207176, RRID: AB_2827968, Abcam) and rabbit anti-beta III Tubulin (1:3000, Cat# ab18207, RRID: AB_1523206, Abcam) overnight at room temperature. To assess angiogenesis, the nerve samples were incubated with rabbit anti-CD31 (1:1000, Cat# ab28364, RRID: AB_726362, Abcam) and rabbit anti-α-smooth muscle actin (α-SMA; 1:1000, Cat# ab202509, RRID: AB_2868435, Abcam) overnight at room temperature. CD31-positive sites were found in the blood vessels and the lumen of mature blood vessels was positive for both CD31 and α-SMA. The sections were subsequently incubated with Cy3-labeled goat anti-rabbit IgG (1:1000, Cat# 33108ES60, Yeason) or FITC-labeled goat anti-rabbit IgG (1:1000, Cat# 33107ES60, Yeason) secondary antibodies for 1 hour at room temperature. Finally, nuclei were stained by 4,6-diamidino-2 phenylindole (DAPI) (Yeason). Immunofluorescence was visualized and captured with a laser confocal microscope (Axio-Imager M2, Zeiss, Jena, Germany).

Histological staining

Two- and four-weeks post-surgery, rats were sampled after anesthesia was induced by intraperitoneal injection with pentobarbital sodium (0.05 mg/g body weight). To observe the histology of nerves, the samples were fixed, dehydrated and embedded in paraffin. Cross-sections or longitudinal sections of the embedded samples were initially stained with hematoxylin and eosin (H&E), Luxol fast blue or toluidine blue to observe the status of the myelin sheaths around the axons. Samples of the gastrocnemius muscle from the injured side were treated similarly and the paraffin-embedded tissue was cut into 7-μm-thick sections before staining with H&E and Masson trichrome stains (Solibor, Beijing, China).

Walking track analysis

Two or four weeks postoperatively, the generally accepted method, sciatic function index (SFI), was calculated to evaluate the functional recovery. As described previously (Yuan et al., 2020), the feet of each rat were dipped in red ink and each rat was placed on a track and their footprints were recorded. Then, the following formula was used for calculating the SFI score:

$$SFI = -38.3 \times (EPL - NPL)/NPL + 109.5 \times (ETS - NTS)/NTS + 13.3 \times (EIT - NIT)/NIT - 8.8,$$

where EIT represents experimental intermediary toe spread (the distance between the second and fourth toes), NIT represents normal intermediary toe spread, ETS represents experimental toe spread (the distance between the first and fifth toes), NTS represents normal toe spread, EPL represents experimental paw length, and NPL represents normal print length.

Target muscle evaluation

Six rats were taken from each group 2 and 4 weeks after surgery (Lee et al., 2020) and anesthetized by intraperitoneal injection of pentobarbital sodium (0.05 mg/g body weight). The three important muscles of the lower limbs (the gastrocnemius muscle, soleus muscle and anterior tibialis muscle) were manually separated, each in their entirety and the ratios of their wet weight (injury side/control side) were calculated. Photographs of muscle fibers were analyzed quantitatively using Image-Pro Plus 4.5 software (Media Cybernetics, Silver Spring, MD, USA). For every sample, five random fields were observed. The muscle fiber's cross-sectional area was calculated with the following equation: $P_m = A_m/A_t \times 100\%$, where A_m represents the muscle fiber area, and A_t represents total field area (Wang et al., 2011). The collagen fibers were stained with Masson trichrome staining kit and their cross-sectional areas (CSA) were assessed using a similar method (Wang et al., 2011).

Neural electrophysiological examination

As previously described (Zhu et al., 2015), after the rats were anesthetized with pentobarbital sodium (0.05 mg/g body weight), the electrophysiology of the sciatic nerves was recorded at 4 weeks after surgery. Briefly, the electrodes were placed superficially beneath the sciatic nerve trunk. To record the compound motor action potential of the bilateral sciatic nerve, a nerve conduction study system (PowerLab, Sydney, Australia) was used to obtain the action potential data amplitude from the curve. Data from the right uninjured sciatic nerve was used for comparison.

Transmission electron microscopy

Four weeks postoperatively, three rats from each group were anesthetized by intraperitoneal injection with pentobarbital sodium (0.05 mg/g body weight). A transmission electron microscopy (TEM, Olympus, Tokyo, Japan) scan was conducted to evaluate the remyelination of the crushed sciatic nerve. First, nerve specimens were fixed in 2% PBS-buffered osmium tetroxide glutaraldehyde for 2 hours at 4°C. The specimens were passed through an ethanol gradient to dehydrate them before infiltration with an epoxy resin and transverse embedding. An ultra-microtome (Leica, Wetzlar, Germany) was used to prepare ultrathin sections (50 nm). These sections were put on copper grids and stained with lead citrate prepare them for TEM examination. In the captured images, the mean diameter of the regenerated myelinated nerve fibers and the fiber density of the myelinated nerve were recorded and calculated.

Western blot assay

Four weeks postoperatively, the rats were sacrificed with excess carbon dioxide inhalation. Briefly, after providing a normal supply of air or oxygen, the concentration of CO_2 was continuously increased until respiratory and cardiac arrest. The CO_2 replacement rate was 30–70%, which ensured that the rats lost consciousness prior to the onset of pain. The intervention time of CO_2 was 35 minutes. The sciatic nerves were then harvested from each group for western blot detection. Briefly, whole protein lysates were obtained, and the protein samples were loaded on sodium dodecyl sulfate polyacrylamide gel and electrophoresis was used for their separation. They were then transferred on to polyvinylidene difluoride membranes (Merck Millipore, Billerica, MA, USA) and incubated with primary rabbit antibodies against von Willebrand factor (1:1000, Cat# ab6994, RRID: AB_11211594, Abcam) and rabbit anti-CD34 (1:1000, Cat# ab81289, RRID: AB_10771056, Abcam) overnight at room temperature. After incubation with goat anti-rabbit secondary antibodies (1:10,000, Cat# ab205718, RRID: AB_10762957, Abcam) the target proteins' relative expression levels were quantified with Quantity One software (Bio Rad Laboratories, Hercules, CA, USA). The protein expression levels were normalized by a β-actin reference sample (rabbit, 1:1000, Cat#

30102ES60, RRID: AB_2728738, Yeason).

Statistical analysis

No statistical methods were used to predetermine sample sizes; however, our sample sizes were similar to those reported in a previous publication (Zhu et al., 2015). No animals or data points were excluded from the analysis. The evaluator was blind to the grouping. SPSS 23.0 software (IBM, Armonk, NY, USA) was used to perform statistical analysis. Data are stated as the mean ± standard deviation (SD). Statistical analysis was by an unpaired Student's *t*-test. $P < 0.05$ was considered to indicate statistical significance in all analyses.

Results

Fabrication and characterization of bioactive hydrogel

The fabrication process of the composite hydrogel is shown in **Figure 2A**. After irradiation for 20 seconds by ultraviolet light, the uncrosslinked GelMA solution formed a GelMA composite hydrogel (**Figure 2B**). The uncrosslinked solution had good fluidity, which meant that it could be directly administered to the injured site and then form a bioactive cumulative-releasing hydrogel by UV irradiation. After freeze drying, we observed the microstructures of both uncrosslinked and crosslinked GelMA. Both had a porous-connected structure (**Figure 2C**), which is advantageous for cell adhesion and nutrient exchange. The Fourier transform infrared spectroscopy spectrum of uncrosslinked GelMA was similar to that of crosslinked GelMA (**Figure 2D**). The degeneration and swelling properties of the GelMA hydrogel and VEGF@GelMA hydrogel were also evaluated. As shown in **Figure 2E**, the degeneration rate of the VEGF@GelMA hydrogel in collagenase-2 solution was slightly lower than that of the GelMA hydrogel. The swelling ratios of these two hydrogels were very similar (**Figure 2F**), which indicates that the incorporation of VEGF did not influence the capacity of the GelMA hydrogel to absorb water. As shown in **Figure 2G**, a sustained release of VEGF could be achieved with the VEGF@GelMA hydrogel, avoiding a burst release of VEGF and facilitating its subsequent *in vitro* or *in vivo* applications.

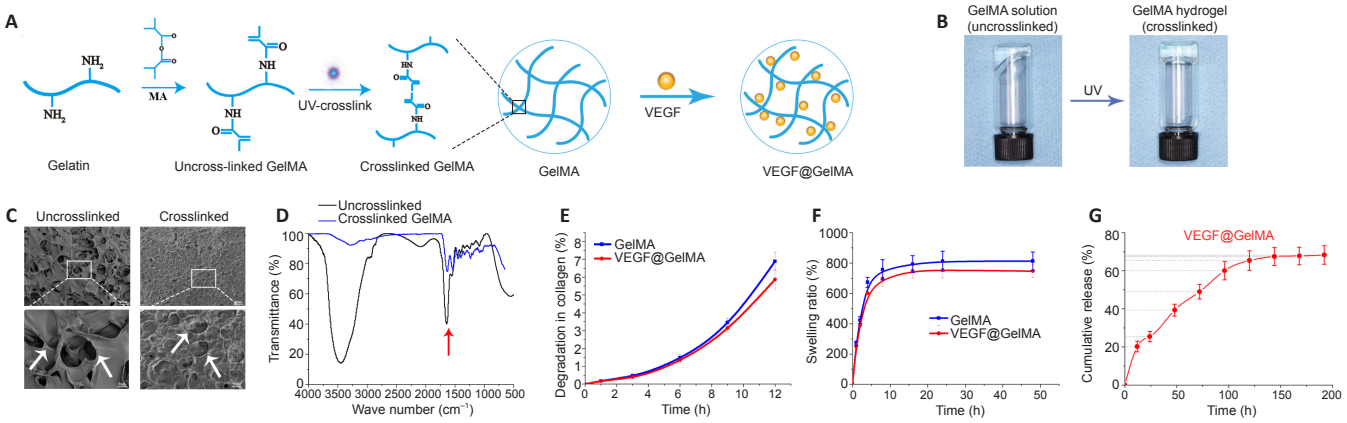

Figure 2 | VEGF@GelMA hydrogel characterization and fabrication.

(A) Flow chart of VEGF@GelMA hydrogel fabrication. (B) Photographs of GelMA solution and its hydrogel after UV treatment. (C) SEM images of uncrosslinked and crosslinked GelMA showed that both hydrogels had porous structures (white arrows). Scale bars: 200 μm (upper), 50 μm (lower). (D) FITR results of uncrosslinked and crosslinked GelMA. The red arrow indicates similar characteristic peaks. (E) Degradation percentage of GelMA and VEGF@GelMA hydrogels. (F) Swelling curve of GelMA and VEGF@GelMA hydrogels. (G) Cumulative release kinetics of VEGF from the VEGF@GelMA hydrogel ($n = 3$). Data are expressed as mean ± SD. The experiment was repeated three times. FITR: Fourier transform infrared spectroscopy; GelMA: gelatin modified by methacrylic anhydride; SEM: scanning electron microscope; UV: ultraviolet; VEGF: vascular endothelial growth factor.

Biocompatibility of the VEGF@GelMA hydrogel

Cell adhesion, cell morphology and growth status were the basic parameters for assessing the biocompatibility of the hydrogel (Liu et al., 2021). Initially, we cultured RSC96 cells in the VEGF@GelMA hydrogel using a three-dimensional culture. After culturing for 10 days, the RSC96 cells grew more with higher density and longer stretches in the VEGF@GelMA hydrogel than on tissue culture polystyrene (TCP), as indicated by phalloidin staining (**Figure 3A**). To further evaluate the bioactivity of the composite hydrogel, HUVECs were seeded on the surface of the hydrogel. As shown in **Figure 3B**, compared with TCP group, many more tubular structures could be observed in the VEGF@GelMA group, which suggested a proangiogenic effect of the bioactive hydrogel *in vitro*.

Establishment of a crush injury model of the rat sciatic nerve

The chronological diagram of *in vivo* animal experiments is shown in **Figure 4A**. To test the bioactivity of the VEGF@GelMA hydrogel *in vivo*, we first established the rat sciatic nerve crush injury model, which is widely used to study the regeneration of the PNS (Varejão et al., 2004; Lee et al., 2020). Briefly, crush injury with hemostatic forceps broke down the internal axons and surrounding myelin sheaths but preserved the epineurium and basal lamina. Then, PBS or the hydrogel was directly administered intra-epineurium to the crushed nerve and surrounding tissues with a microsyringe (**Figure 4B**). The crush effects were confirmed through functional and histological analysis. After the nerve crush, the SFI score decreased ($P < 0.01$; **Figure 4C**). The histological staining (H&E, toluidine blue and Luxol fast blue) results showed that the distance between the epineurium in the crushed group was considerably narrower than that in the normal sciatic nerve group (**Figure 4D**), indicating a successful establishment of the rat sciatic nerve crush injury model.

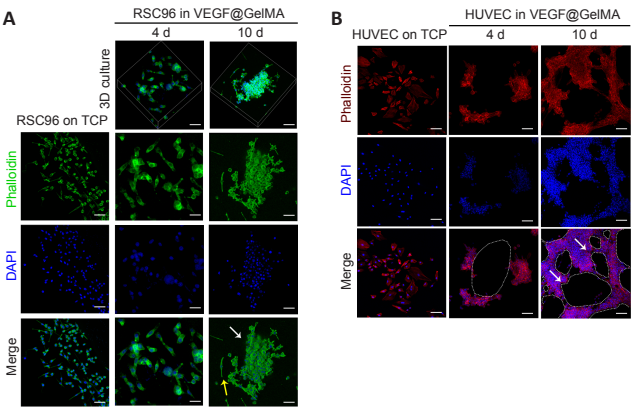

Figure 3 | Biocompatibility of the VEGF@GelMA hydrogel detected by RSC96 cells and HUVECs.

(A) Microfilament skeleton of RSC96 cells cultured in VEGF@GelMA hydrogel for 4 and 10 days stained by phalloidin staining (green). RSC96 cells grew better with higher density (white arrow) and in longer stretches (yellow arrow) in the VEGF@GelMA hydrogel. (B) HUVECs were cultured on the surface of the VEGF@GelMA hydrogel for 4 and 10 days stained by phalloidin staining (red). More tubular structures (white arrow) could be observed in the VEGF@GelMA group. Scale bars: 50 μm. 3D: Three-dimensional; DAPI: 2-(4-amidinophenyl)-6-indolecarbamidine dihydrochloride; GelMA: gelatin modified by methacrylic anhydride; HUVEC: human umbilical vein endothelial cell; TCP: tissue culture polystyrene; VEGF: vascular endothelial growth factor.

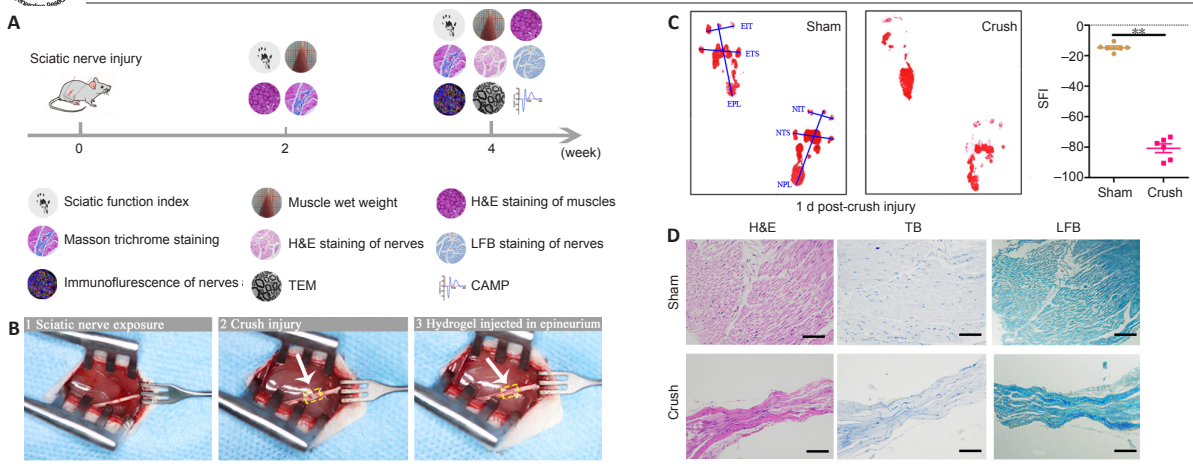

Figure 4 | **Establishment of the sciatic nerve crush injury rat model.**
(A) The diagram of the procedures used in animal experiments *in vivo*. (B) The rat sciatic nerve was exposed, crushed and then injected with bioactive hydrogel. The white arrow indicated the crushed site. (C) SFI analysis of rats in the sham and crush groups 1 day postoperatively. Data are expressed as mean ± SD (n = 6). $^{**}P < 0.01$ (unpaired Student's t-test). (D) Histological staining (H&E, TB and LFB staining) showed the crushed nerve fibers in the Crush group. The yellow arrows indicate the crushed nerves. Scale bars: 100 μm. CAMP: Compound motor action potential; GelMA: gelatin modified by methacrylic anhydride; H&E: hematoxylin and eosin; LFB: Luxol fast blue staining; SFI: sciatic function index; TB: toluidine blue; TEM: transmission electron microscopy.

Effect of bioactive hydrogel on muscle functional recovery in a sciatic nerve crush injury rat model

The *in vitro* data demonstrated the good biocompatibility and excellent bioactivity of the VEGF@GelMA hydrogel, but *in vivo* studies were necessary to comprehensively evaluate the outcomes of the composite hydrogel regarding PNS repair. Two and four weeks after surgery, the SFI score was considerably higher in the crush + VEGF@GelMA group than in both the crush + PBS and crush + GelMA groups (both $P <$ 0.05; **Figure 5A** and **B**). Target muscle analysis showed that the wet ratios of the gastrocnemius muscle, soleus muscle and anterior tibialis muscle in the crush + VEGF@GelMA group were considerably higher compared with those in the other two groups ($P < 0.05$; **Figure 5C** and **D**). This result indicated that the sustained delivery of VEGF reduced the atrophy of the three target muscles that were innervated by the injured sciatic nerve. H&E and Masson trichrome staining were used for histological analyses of the effect of VEGF on denervated muscular atrophy (**Figure 5E–H**). Four weeks postoperatively, the cross-sectional area of muscle fibers was significantly higher in the crush + VEGF@GelMA group than in the crush + PBS ($P < 0.01$) and crush + GelMA ($P <$ 0.05) groups (**Figure 5F**). However, the average percentage of collagen fiber area in the crush + VEGF@GelMA group was more pronounced than those in the crush + GelMA ($P < 0.01$) and crush + PBS groups ($P < 0.05$; **Figure 5H**). All these data indicated that the denervation of target muscles and muscle atrophy resulting from crush injury could be attenuated by VEGF@GelMA hydrogel injection therapy.

Effect of hydrogel on nerve regeneration in a sciatic nerve crush injury rat model

Nerve repair 4 weeks post crush injury was determined through histological and electrophysiological examinations. Representative images of H&E staining and Luxol fast blue staining of the four groups are displayed in **Figure 6A** and **B**. These results indicated that more axonal regeneration and remyelination developed in the crush + VEGF@GelMA group compared with the other crush groups, however, the nerve fibers were better organized in the sham group. Furthermore, we evaluated axonal regrowth and nerve remyelination through immunofluorescence assays using four critical markers, S100β, neurofilament-200, beta III Tubulin and myelin basic protein. Neurofilament-200 and beta III Tubulin indicated regenerated axons and neurofilaments, whereas the expression of S100β and myelin basic protein are measures of axonal remyelination status (Cattin et al., 2015; Fan et al., 2018). **Figure 6C** and **D** show that the levels of these indicators were stronger in the crush + VEGF@GelMA group than those in the crush + PBS and crush + GelMA groups. These data suggested that VEGF@GelMA promoted nerve regeneration after 4 weeks of administration.

TEM was used to evaluate the axons and their remyelination of regenerated nerve fibers. Representative images of the middle segment of each nerve sample are displayed in **Figure 7A**. At 4 weeks post-injury, some myelinated axons had developed in the crush + PBS groups that suggested Wallerian degeneration of the sciatic nerve in contrast to the uniform structure bounded by electron-dense, clear and thick myelin sheaths observed in the sham group. Quantitative analysis parameters (including myelin thickness, myelinated axons diameter and myelinated axons percentage) were also used to assess regenerative efficacy. All values of the above three parameters were highest in the crush + VEGF@GelMA group compared with the values in the crush + PBS and crush + GelMA groups ($P < 0.05$ or $P < 0.01$; **Figure 7B–D**). Electrophysiology of neurons accurately quantifies nerve function (Lu et al., 2019). In our study, the compound motor action potential amplitude in the crush + VEGF@GelMA group was higher than in either the crush + PBS ($P < 0.01$) or crush + GelMA groups ($P < 0.05$; **Figure 7E** and **F**), also indicating that repair of the crushed nerve is accelerated when using the bioactive hydrogel.

The composite hydrogel benefits the recovery of vascularization in a sciatic nerve crush injury rat model

In tandem with our evaluations of neuronal regeneration, we studied vascularization improvement after VEGF@GelMA hydrogel injection into the injury site. CD31 is widely involved in the angiogenesis process and may act through modulating the intercellular junctions of endothelial cells (Cattin et al., 2015). The results of CD31 immunofluorescence staining suggested significantly more formation of microvessels in the crush + VEGF@GelMA group compared with the other three groups ($P < 0.05$; **Figure 8A** and **B**). The presence of α-SMA indicates that the neovascular tissues progress become into mature vessels (Guan et al., 2021). The α-SMA-positive mature vessel density was also considerably higher in the crush + VEGF@GelMA group compared with either the crush + PBS or crush + GelMA groups ($P < 0.05$; **Figure 8A** and **C**), which indicated that VEGF delivery promoted vessel maturation. Consistent with this, the protein expression of CD34 and von Willebrand factor (important factors associated with vascular tissues) (Abdulkadir et al., 2020) measured by western blot further confirmed the proangiogenic effects of the VEGF@GelMA hydrogel (**Figure 8D** and **E**). These data showed that controlled release of VEGF from the bioactive hydrogel promoted vascularization, which may provide nutrients, remove waste and facilitate nerve regeneration synergistically.

Discussion

Nerve crush injury often results from acute blunt-force trauma, causing severe compression of the nerve trunk or its branches. Currently, there are only a few clinical strategies for the treatment of nerve crush injury and they mainly involve the supplementation of neurotrophic factors, primarily nerve growth factor. However, the therapeutic efficacy is limited due to the low effective drug concentration that reaches the injured region. With the rapid development of microsurgery technologies, intraepineurium injection offers a promising alternative (Manoukian et al., 2020; Lopez-Silva et al., 2021). Recently, Masgutov et al. (2021) injected the plasmid construct pBud-coVEGF165-coGFG2 into the epineurium of the rat sciatic nerve and found that local administration of the composite plasmid could act as a proangiogenic stimulus and facilitate regeneration of the sciatic nerve. Consistent with this, our results collectively showed that direct injection of VEGF-released hydrogel could accelerate nerve regeneration after crush injury; therefore, it may be a beneficial option for nerve crush injury treatment.

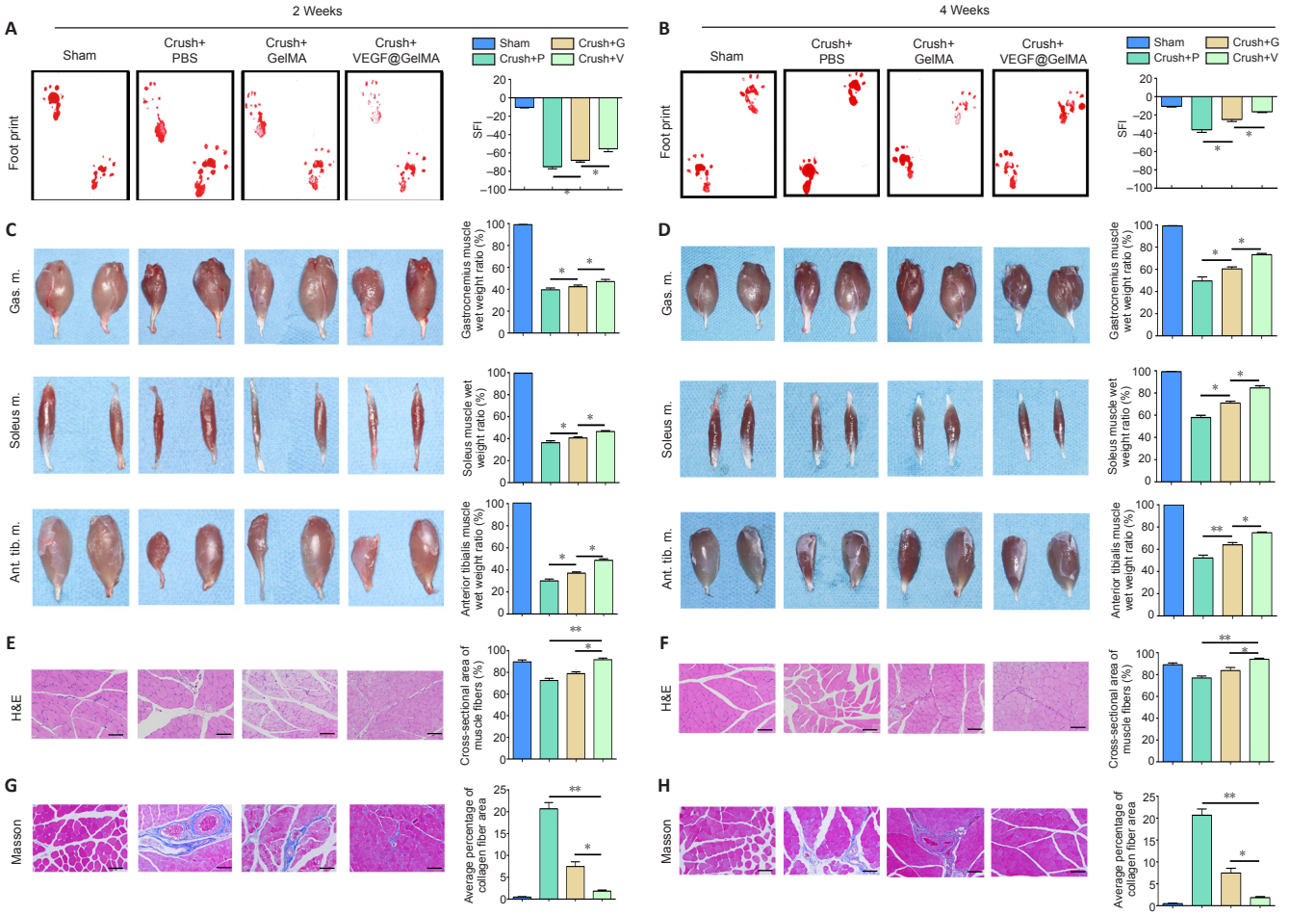

Figure 5 | **Functional recovery of crushed sciatic nerves after VEGF@GelMA injection at 2 and 4 weeks after sciatic nerve injury.**
(A, B) Representative images of footprints in the four groups and corresponding SFI analysis at 2 (A) or 4 weeks (B) after surgery. The footprints were more relaxed in the Crush+VEGF@GelMA group than the other crush groups. (C, D) Gross view of gastrocnemius muscles, soleus muscles and anterior tibialis muscles in all groups and corresponding wet weight ratio analysis at 2 (C) or 4 weeks (D) after surgery. The atrophic degree of denervated muscles was alleviated in the Crush + VEGF@GelMA group. The yellow arrows indicated the innervated muscles. (E, F) Representative H&E staining images of gastrocnemius muscles and corresponding CSA of muscle fibers at 2 (E) or 4 weeks (F) after surgery. (G, H) Representative Masson's trichrome staining images of the gastrocnemius muscles and corresponding average percentage of collagen fiber area at 2 (G) or 4 weeks (H) after surgery. The CSA of muscle fibers was highest in Crush + VEGF@GelMA group, while the average percentage of collagen fiber was lowest. Scale bars: 5 mm in A–D, 100 μm in E–H. Data are expressed as mean ± SD (n = 6). *P < 0.05, **P < 0.01 (unpaired Student's t-test). Ant. Tib. m.: Anterior tibial muscle; Crush + V: Crush + VEGF@GelMA group; Crush+G: Crush + GelMA group; Crush+P: Crush + PBS group; CSA: cross sectional area; Gas. m.: Gastrocnemius muscle; GelMA: gelatin modified by methacrylic anhydride; H&E staining: hematoxylin-eosin staining; SFI: sciatic function index; Soleus. m.: soleus muscle; VEGF: vascular endothelial growth factor.

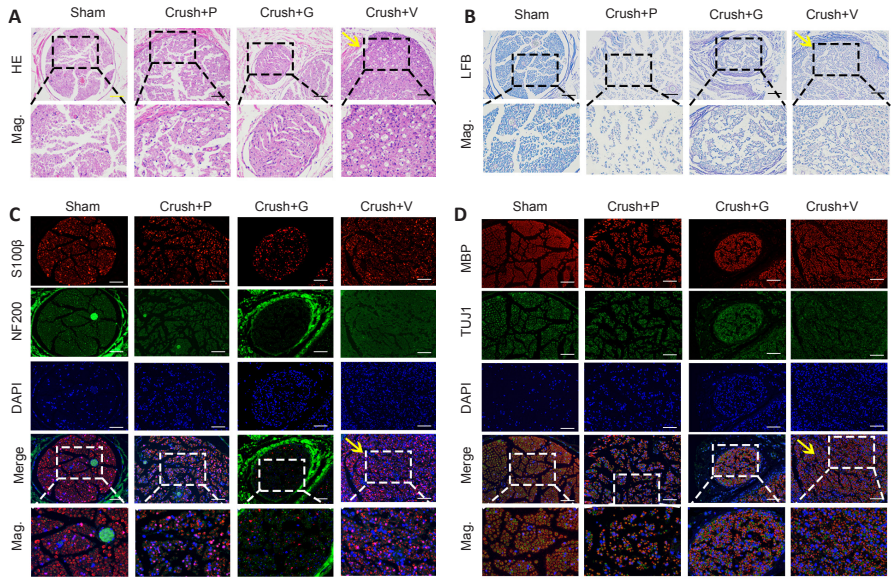

Figure 6 | **Histological analysis of sciatic nerves 4 weeks after hydrogel injection *in vivo*.**
(A) H&E staining of regenerated nerves. (B) LFB staining of regenerated nerves. (C) Triple immunofluorescent staining of S100β (Cy3-red, an indicator for myelin or Schwann cells), NF200 (FITC-green, an indicator for axons) and DAPI (nuclei) was performed. (D) Triple immunofluorescent staining of MBP (Cy3-red, an indicator for myelin or Schwann cells), TUJ1 (FITC-green, an indicator for axons) and DAPI was performed. VEGF@GelMA promoted nerve regeneration after 4 weeks of administration. The yellow arrows indicated the best nerve regeneration formed in the Crush + V group. Scale bars: 100 μm. Crush+G: Crush + GelMA group; Crush+P: crush + PBS group; Crush+V: crush + VEGF@GelMA group; DAPI: 2-(4-amidinophenyl)-6-indolecarbamidine dihydrochloride; FITC: fluoresceine isothiocyanate; GelMA: gelatin modified by methacrylic anhydride; H&E: hematoxylin and eosin; LFB: Luxol fast blue staining; Mag.: magnification; MBP: myelin basic protein; NF200: neurofilament-200; TUJ1: β-tubulin III; VEGF: vascular endothelial growth factor.

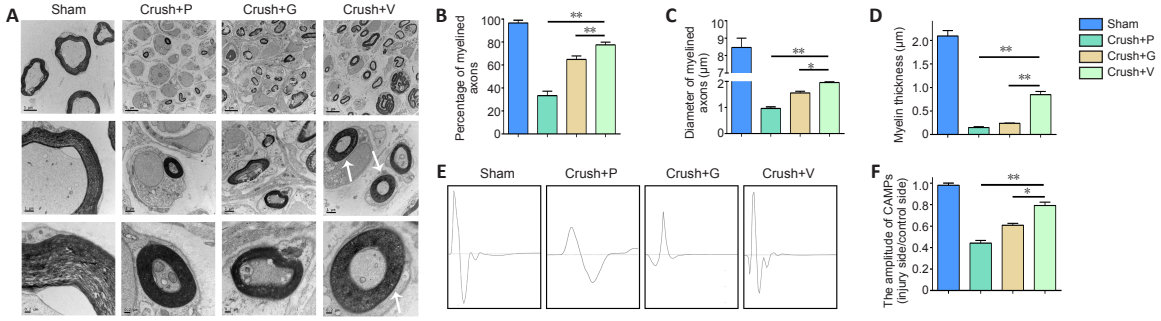

Figure 7 | **Crushed sciatic nerves show differential myelination and electrophysiological performance after hydrogel administration.**
(A) Representative TEM images of cross-sections at different magnifications. Compared with Crush + P and Crush + G groups, more myelinated axons and thicker myelin (white arrows) were formed in the Crush + V group. Scale bars: 5 μm (upper), 1 μm (middle), 0.2 μm (lower). (B–D) Quantification of myelinated axons percentage (B), myelinated axon diameter (C) and myelin thickness (D). (E) CMAP representative images. The amplitude of CAMP in the Crush + V group was significantly higher than the other two groups. (F) Quantification of CAMP amplitude. Data are expressed as mean ± SD (n = 3). *$P < 0.05$, **$P < 0.01$ (unpaired Student's *t*-test). CAMP: Compound motor action potential; Crush+G: Crush + GelMA group; Crush+P: Crush + PBS group; Crush+V: Crush + VEGF@GelMA group; GelMA: gelatin modified by methacrylic anhydride; TEM: transmission electron microscope; VEGF: vascular endothelial growth factor.

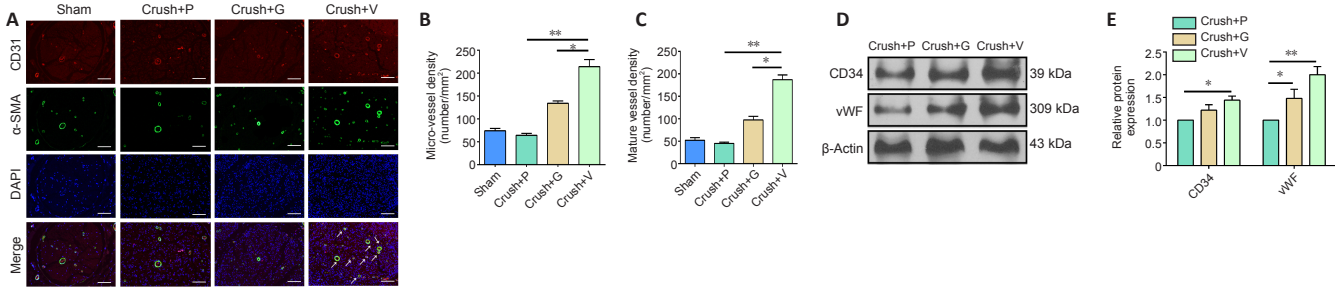

Figure 8 | **VEGF@GelMA hydrogel promotes angiogenesis of regenerated nerves.**
(A) CD31 (Cy3-red, an indicator for blood vessel structures) and α-SMA (FITC-green, an indicator for mature blood vessels) staining of regenerated nerves showed the Crush+V group developed the most mature vessels (white arrows) . DAPI (blue) was used for staining nuclei. Scale bars: 100 μm. (B, C) Quantification of microvessel density (B), mature vessel density (C). (D) Western blot detection of CD34 and vWF in regenerated nerves at 4 weeks post-operatively showed higher protein expression of CD34 and vWF in the Crush + V group. (E) Quantification of CD34 and vWF expression. The relative expression was normalized by β-actin. Data are expressed as mean ± SD ($n = 3$). *$P < 0.05$, **$P < 0.01$ (unpaired Student's *t*-test). Crush+G: Crush + GelMA group; Crush+P: crush + PBS group; Crush+V: crush + VEGF@GelMA group; DAPI: 2-(4-amidinophenyl)-6-indolecarbamidine dihydrochloride; GelMA: gelatin modified by methacrylic anhydride; VEGF: vascular endothelial growth factor; vWF: von Willebrand factor; α-SMA: alpha-smooth muscle actin.

In the present study, we first fabricated a photocrosslinkable GelMA hydrogel with controlled release of VEGF. Its physical properties and biocompatibility were investigated both *in vitro* and *in vivo*. The GelMA hydrogel has attracted the attention of numerous researchers because its three-dimensional network structure could serve as an optimal microenvironment for cell adhesion, proliferation and migration. In addition, GelMA could act as an excellent carrier of biochemical or genetic cues for peripheral nerve repair (Xu et al., 2020; Sultan et al., 2021). Zhuang et al. (2016) synthetized glial cell line-derived neurotrophic factor-loaded microspheres and these GelMA hydrogel-seeded microspheres served as a new biodegradable artificial nerve guide. Consistent results were also reported, demonstrating that a third-generation nerve regeneration conduit (based on GelMA hydrogel and dental pulp stem cells) was an improved tissue engineering method that could replace traditional nerve autografts when treating large gap defects after peripheral nerve injuries (Luo et al., 2021). Our experiment validated the beneficial use of GelMA hydrogel in nerve repair of crush injury and should broadened the application of this type of bioactive hydrogel.

Anatomically, peripheral nerves are composed of nervous tissue, structures supporting connective tissue and blood vessels to supply nutrients. The nervous system and the vascular system share similar signaling pathways and anatomical structures (Mukouyama et al., 2002) and the crosstalk between the two systems is considered to be quite critical in both tissue development and regeneration, including in the repair of PNI (Zhu et al., 2015; Wang et al., 2017). It has also been shown that freshly developed blood vessels direct Schwann cell migration and promote peripheral nerve axon regrowth (Cattin et al., 2015). However, the establishment and maturation of angiogenesis requires more than 3 weeks (Hoefer et al., 2001). Thus, a bioactive platform with sustained long-term (over a physiologically relevant timeframe) proangiogenic abilities is needed. Our results confirmed that a sustained release of VEGF could be achieved through its incorporation into the GelMA hydrogel. This VEGF@GelMA hydrogel facilitated the adhesion and proliferation of HUVECs *in vitro* and enhanced the formation of mature blood vessels in a nerve crush injury model. Bin et al. (2020) constructed a revascularized nerve graft that depended on a VEGF-heparin sustained release system. They found that tissue-engineered peripheral nerves could restore the blood supply, which greatly advanced the repair of peripheral nerve defects (Bin et al., 2020). Consistent with this, our unique VEGF@GelMA system with endoneural administration accelerated the peripheral nerve regeneration, which was linked to increased blood vessel formation in the regenerated nerves.

Apart from the direct use of growth factors, it has been demonstrated that VEGF gene therapies could increase the number of myelinated fibers, increase gastrocnemius weight and improve SFI scores after sciatic nerve transection (Pereira Lopes et al., 2011; Masgutov et al., 2021). Others concluded that dual delivery of plasmid VEGF and nerve growth factor as gene therapy may enhance sciatic nerve regeneration (Fang et al., 2020). In our experiment, a single administration of VEGF@GelMA hydrogel at the time of surgical sciatic nerve crush facilitated the nerve regeneration and functional recovery and would preclude the hinderances and risks associated with gene therapy. Additionally, VEGF-mimicking peptide has been discussed in recent studies (Leslie-Barbick et al., 2011; Dmytriyeva et al., 2020). Lu et al. (2019) and showed that brain-derived neurotrophic factor- and VEGF-mimetic peptides synergistically facilitate the process of nerve regeneration. Notably, it was found that an aligned chitosan fiber hydrogel grafted with RGI (Ac-RGIDKRHWNSQGG, a brain-derived neurotrophic factor-mimicking peptide)/KLT (Ac-KLTWQELYQLKYKGIGG, a VEGF-mimicking peptide) offered an efficient way for sciatic nerve defect repair (Rao et al., 2020). The merits of these peptides are primarily reduced costs, ease of design and synthesis and self-assembly behavior. So far, however, there have been no direct comparative studies between growth factors and their mimetic peptides and this warrants further exploration.

There are several limitations to this research. First, the VEGF family contains several different isoforms, such as VEGF-A and VEGF-B. Only VEGF165 (a version of VEGF-A) was studied in this research; therefore, the specific role of other isoforms in peripheral nerve regeneration should be clarified. Second, the *in vitro* studies preliminarily demonstrated that the fabricated hydrogel supported cell adhesion and growth of RSC96 and HUVECs. However, both cell types aggregate easily over the 10-day culture period. The interesting phenomenon and inherent mechanism need further explanations. Other *in vitro* experiments (including three-dimensional culture of HUVEC, CD31 staining for HUVEC and S100β staining for RSC96) would enhance the display of the real status of these seed cells in the hydrogel. Another limitation is that the evaluation of angiogenesis in this study used basic methods of immunofluorescence and western blot, therefore, micro-CT angiography analysis and other methods could be included. Furthermore, more strategies could be adopted to prolong the release timeframe of the functional growth factors or drugs, to discover the maximal effect on nerve repair. Investigation of the specific molecular mechanisms behind the vascularization–neurogenesis crosstalk should lead to other treatment options.

In the current study, we fabricated a crosslinked bioactive hydrogel (VEGF@GelMA) with nerve regeneration-facilitating and proangiogenic characteristics. The controlled release of VEGF from the composite hydrogel accelerated neurite regeneration, axonal remyelination and revascularization of crushed sciatic nerves. Our results show that the VEGF@GelMA hydrogel offers a new option and offers a great possibility for the clinical treatment of peripheral nerve crush injury.

Author contributions: *Study design: WY, JY; experiment implementation: WX, YW; data analysis: HL, WX, YZ; manuscript preparation: HL; manuscript writing: WX, YZ; constructive discussion and manuscript revision: WY, JY. All authors read and approved the final version of the manuscript.*
Conflicts of interest: *The authors declare no conflict of interests.*

Open peer reviewer: *Alonzo D. Cook, Brigham Young University, USA.*

References

Abdulkadir RR, Alwjwaj M, Othman OA, Rakkar K, Bayraktutan U (2020) Outgrowth endothelial cells form a functional cerebral barrier and restore its integrity after damage. Neural Regen Res 15:1071-1078.
Ahmed MN, Shi D, Dailey MT, Rothermund K, Drewry MD, Calabrese TC, Cui XT, Syed-Picard FN (2021) Dental pulp cell sheets enhance facial nerve regeneration via local neurotrophic factor delivery. Tissue Eng Part A 27:1128-1139.
Beer GM, Steurer J, Meyer VE (2001) Standardizing nerve crushes with a non-serrated clamp. J Reconstr Microsurg 17:531-534.
Bin Z, Zhihu Z, Jianxiong M, Xinlong M (2020) Repairing peripheral nerve defects with revascularized tissue-engineered nerve based on a vascular endothelial growth factor-heparin sustained release system. J Tissue Eng Regen Med 14:819-828.
Cattin AL, Burden JJ, Van Emmenis L, Mackenzie FE, Hoving JJ, Garcia Calavia N, Guo Y, McLaughlin M, Rosenberg LH, Quereda V, Jamecna D, Napoli I, Parrinello S, Enver T, Ruhrberg C, Lloyd AC (2015) Macrophage-induced blood vessels guide schwann cell-mediated regeneration of peripheral nerves. Cell 162:1127-1139.
Dmytriyeva O, de Diego Ajenjo A, Lundø K, Hertz H, Rasmussen KK, Christiansen AT, Klingelhofer J, Nielsen AL, Hoeber J, Kozlova E, Woldbye DPD, Pankratova S (2020) Neurotrophic effects of vascular endothelial growth factor B and novel mimetic peptides on neurons from the central nervous system. ACS Chem Neurosci 11:1270-1282.
Dursun Usal T, Yucel D, Hasirci V (2019) A novel GelMA-pHEMA hydrogel nerve guide for the treatment of peripheral nerve damages. Int J Biol Macromol 121:699-706.
Fan L, Liu C, Chen X, Zou Y, Zhou Z, Lin C, Tan G, Zhou L, Ning C, Wang Q (2018) Directing induced pluripotent stem cell derived neural stem cell fate with a three-dimensional biomimetic hydrogel for spinal cord injury repair. ACS Appl Mater Interfaces 10:17742-17755.
Fang Z, Ge X, Chen X, Xu Y, Yuan WE, Ouyang Y (2020) Enhancement of sciatic nerve regeneration with dual delivery of vascular endothelial growth factor and nerve growth factor genes. J Nanobiotechnology 18:46.
Ferrara N, Gerber HP, LeCouter J (2003) The biology of VEGF and its receptors. Nat Med 9:669-676.
Flores AJ, Lavernia CJ, Owens PW (2000) Anatomy and physiology of peripheral nerve injury and repair. Am J Orthop (Belle Mead NJ) 29:167-173.
Guaiquil VH, Pan Z, Karagianni N, Fukuoka S, Alegre G, Rosenblatt MI (2014) VEGF-B selectively regenerates injured peripheral neurons and restores sensory and trophic functions. Proc Natl Acad Sci U S A 111:17272-17277.
Guan Y, Gao N, Niu H, Dang Y, Guan J (2021) Oxygen-release microspheres capable of releasing oxygen in response to environmental oxygen level to improve stem cell survival and tissue regeneration in ischemic hindlimbs. J Control Release 331:376-389.
Henry TD, Annex BH, McKendall GR, Azrin MA, Lopez JJ, Giordano FJ, Shah PK, Willerson JT, Benza RL, Berman DS, Gibson CM, Bajamonde A, Rundle AC, Fine J, McCluskey ER, VIVA Investigators (2003) The VIVA trial: Vascular endothelial growth factor in Ischemia for Vascular Angiogenesis. Circulation 107:1359-1365.
Hoefer IE, van Royen N, Buschmann IR, Piek JJ, Schaper W (2001) Time course of arteriogenesis following femoral artery occlusion in the rabbit. Cardiovasc Res 49:609-617.
Hu X, Zhao S, Luo Z, Zuo Y, Wang F, Zhu J, Chen L, Yang D, Zheng Y, Zheng Y, Cheng Y, Zhou F, Yang Y (2020) On-chip hydrogel arrays individually encapsulating acoustic formed multicellular aggregates for high throughput drug testing. Lab on a chip 20:2228-2236.
Kilkenny C, Browne W, Cuthill IC, Emerson M, Altman DG (2011) Animal research: reporting in vivo experiments--the ARRIVE guidelines. J Cereb Blood Flow Metab 31:991-993.
Lee JI, Hur JM, You J, Lee DH (2020) Functional recovery with histomorphometric analysis of nerves and muscles after combination treatment with erythropoietin and dexamethasone in acute peripheral nerve injury. PLoS One 15:e0238208.
Leslie-Barbick JE, Saik JE, Gould DJ, Dickinson ME, West JL (2011) The promotion of microvasculature formation in poly(ethylene glycol) diacrylate hydrogels by an immobilized VEGF-mimetic peptide. Biomaterials 32:5782-5789.
Li A, Pereira C, Hill EE, Vukcevich O, Wang A (2021a) In vitro, in vivo and ex vivo models for peripheral nerve injury and regeneration. Curr Neuropharmacol doi: 10.2174/1570159X19666210407155543.
Li R, Xu J, Rao Z, Deng R, Xu Y, Qiu S, Long H, Zhu Q, Liu X, Bai Y, Quan D (2021b) Facilitate angiogenesis and neurogenesis by growth factors integrated decellularized matrix hydrogel. Tissue Eng Part A 27:771-787.
Lin YJ, Lee YW, Chang CW, Huang CC (2020) 3D spheroids of umbilical cord blood MSC-derived Schwann cells promote peripheral nerve regeneration. Front Cell Dev Biol 8:604946.
Liu J, Zeng H, Xiao P, Yang A, Situ X, Wang Y, Zhang X, Li W, Pan W, Wang Y (2020) Sustained release of magnesium ions mediated by a dynamic mechanical hydrogel to enhance BMSC proliferation and differentiation. ACS Omega 5:24477-24486.
Liu Y, Du J, Peng P, Cheng R, Lin J, Xu C, Yang H, Cui W, Mao H, Li Y, Geng D (2021) Regulation of the inflammatory cycle by a controllable release hydrogel for eliminating postoperative inflammation after discectomy. Bioact Mater 6:146-157.
Lopez-Silva TL, Cristobal CD, Edwin Lai CS, Leyva-Aranda V, Lee HK, Hartgerink JD (2021) Self-assembling multidomain peptide hydrogels accelerate peripheral nerve regeneration after crush injury. Biomaterials 265:120401.
Lu J, Yan X, Sun X, Shen X, Yin H, Wang C, Liu Y, Lu C, Fu H, Yang S, Wang Y, Sun X, Zhao L, Lu S, Mikos AG, Peng J, Wang X (2019) Synergistic effects of dual-presenting VEGF- and BDNF-mimetic peptide epitopes from self-assembling peptide hydrogels on peripheral nerve regeneration. Nanoscale 11:19943-19958.
Luo L, He Y, Jin L, Zhang Y, Guastaldi FP, Albashari AA, Hu F, Wang X, Wang L, Xiao J, Li L, Wang J, Higuchi A, Ye Q (2021) Application of bioactive hydrogels combined with dental pulp stem cells for the repair of large gap peripheral nerve injuries. Bioact Mater 6:638-654.
Manoukian OS, Baker JT, Rudraiah S, Arul MR, Vella AT, Domb AJ, Kumbar SG (2020) Functional polymeric nerve guidance conduits and drug delivery strategies for peripheral nerve repair and regeneration. J Control Release 317:78-95.
Masgutov R, Zeinalova A, Bogov A, Masgutova G, Salafutdinov I, Garanina E, Syromiatnikova V, Idrisova K, Mullakhmetova A, Andreeva D, Mukhametova L, Kadyrov A, Pankov I, Rizvanov A (2021) Angiogenesis and nerve regeneration induced by local administration of plasmid pBud-coVEGF165-coFGF2 into the intact rat sciatic nerve. Neural Regen Res 16:1882-1889.
Mukouyama YS, Shin D, Britsch S, Taniguchi M, Anderson DJ (2002) Sensory nerves determine the pattern of arterial differentiation and blood vessel branching in the skin. Cell 109:693-705.
Pereira Lopes FR, Lisboa BC, Frattini F, Almeida FM, Tomaz MA, Matsumoto PK, Langone F, Lora S, Melo PA, Borojevic R, Han SW, Martinez AM (2011) Enhancement of sciatic nerve regeneration after vascular endothelial growth factor (VEGF) gene therapy. Neuropathol Appl Neurobiol 37:600-612.
Qiao Y, Liu X, Zhou X, Zhang H, Zhang W, Xiao W, Pan G, Cui W, Santos HA, Shi Q (2020) Gelatin templated polypeptide co-cross-linked hydrogel for bone regeneration. Adv Healthc Mater 9:e1901239.
Qin M, Jin J, Saiding Q, Xiang Y, Wang Y, Sousa F, Sarmento B, Cui W, Chen X (2020) In situ inflammatory-regulated drug-loaded hydrogels for promoting pelvic floor repair. J Control Release 322:375-389.
Raimondo TM, Li H, Kwee BJ, Kinsley S, Budina E, Anderson EM, Doherty EJ, Talbot SG, Mooney DJ (2019) Combined delivery of VEGF and IGF-1 promotes functional innervation in mice and improves muscle transplantation in rabbits. Biomaterials 216:119246.
Rao F, Wang Y, Zhang D, Lu C, Cao Z, Sui J, Wu M, Zhang Y, Pi W, Wang B, Kou Y, Wang X, Zhang P, Jiang B (2020) Aligned chitosan nanofiber hydrogel grafted with peptides mimicking bioactive brain-derived neurotrophic factor and vascular endothelial growth factor repair long-distance sciatic nerve defects in rats. Theranostics 10:1590-1603.
Ruijs AC, Jaquet JB, Kalmijn S, Giele H, Hovius SE (2005) Median and ulnar nerve injuries: a meta-analysis of predictors of motor and sensory recovery after modern microsurgical nerve repair. Plast Reconstr Surg 116:484-494; discussion 495-496.
Shvartsman D, Storrie-White H, Lee K, Kearney C, Brudno Y, Ho N, Cezar C, McCann C, Anderson E, Koullias J, Tapia JC, Vandenburgh H, Lichtman JW, Mooney DJ (2014) Sustained delivery of VEGF maintains innervation and promotes reperfusion in ischemic skeletal muscles via NGF/GDNF signaling. Mol Ther 22:1243-1253.
Sultan MT, Choi BY, Ajiteru O, Hong DK, Lee SM, Kim HJ, Ryu JS, Lee JS, Hong H, Lee YJ, Lee H, Suh YJ, Lee OJ, Kim SH, Suh SW, Park CH (2021) Reinforced-hydrogel encapsulated hMSCs towards brain injury treatment by trans-septal approach. Biomaterials 266:120413.
Sunderland S (1951) A classification of peripheral nerve injuries producing loss of function. Brain 74:491-516.
Varejão AS, Cabrita AM, Meek MF, Bulas-Cruz J, Melo-Pinto P, Raimondo S, Geuna S, Giacobini-Robecchi MG (2004) Functional and morphological assessment of a standardized rat sciatic nerve crush injury with a non-serrated clamp. J Neurotrauma 21:1652-1670.
Wang CY, Zhang KH, Fan CY, Mo XM, Ruan HJ, Li FF (2011) Aligned natural-synthetic polyblend nanofibers for peripheral nerve regeneration. Acta Biomater 7:634-643.
Wang H, Zhu H, Guo Q, Qian T, Zhang P, Li S, Xue C, Gu X (2017) Overlapping mechanisms of peripheral nerve regeneration and angiogenesis following sciatic nerve transection. Front Cell Neurosci 11:323.
Xu H, Sun M, Wang C, Xia K, Xiao S, Wang Y, Ying L, Yu C, Yang Q, He Y, Liu A, Chen L (2020) Growth differentiation factor-5-gelatin methacryloyl injectable microspheres laden with adipose-derived stem cells for repair of disc degeneration. Biofabrication 13:015010.
Xu WL, Ong HS, Zhu Y, Liu SW, Liu LM, Zhou KH, Xu ZQ, Gao J, Zhang Y, Ye JH, Yang WJ (2017) In situ release of VEGF enhances osteogenesis in 3D porous scaffolds engineered with osterix-modified adipose-derived stem cells. Tissue Eng Part A 23:445-457.
Yuan YS, Niu SP, Yu F, Zhang YJ, Han N, Lu H, Yin XF, Xu HL, Kou YH (2020) Intraoperative single administration of neutrophil peptide 1 accelerates the early functional recovery of peripheral nerves after crush injury. Neural Regen Res 15:2108-2115.
Zhu Y, Liu S, Zhou S, Yu Z, Tian Z, Zhang C, Yang W (2015) Vascularized versus nonvascularized facial nerve grafts using a new rabbit model. Plast Reconstr Surg 135:331e-339e.
Zhuang H, Bu S, Hua L, Darabi MA, Cao X, Xing M (2016) Gelatin-methacrylamide gel loaded with microspheres to deliver GDNF in bilayer collagen conduit promoting sciatic nerve growth. Int J Nanomedicine 11:1383-1394.

P-Reviewer: Cook AD; C-Editor: Zhao M; S-Editors: Yu J, Li CH; L-Editors: Yu J, Song LP; T-Editor: Jia Y